약학석사학위논문

Lymph node-targeting and antigen-presenting proteinticles for *in vivo* cancer immunotherapy

림프절 표적형, 항원 제시형 단백질 나노입자를 이용한 암 면역 치료법

2015년 8월

서울대학교 융합과학기술대학원

분자의학 및 바이오제약학과

고 호 경

ABSTRACT

Cancer immunotherapy is a new class of cancer treatment which uses the body's own immune system to defeat cancers. To elicit immune responses that attack cancer cells, efficient antigen delivery to lymph nodes (LNs) can be an appropriate strategy, because LNs possess a high population of immune-related cells such as antigen presenting cells (APCs), T cells and B cells. However, realization of this strategy remains challenging. Biocompatible protein-based nanoparticles (named "proteinticles") that self-assemble inside cells with precise 3D nanostructure, have a unique advantage over synthetic nanomaterials for LN-targeting immunotherapy. Herein, human ferritin heavy chain (HFt) and red fluorescence protein (RFP) were selected as a promising antigen carrier and a model antigen, respectively. Genetically recombined HFt-RFP vaccine particle with a size of 26 nm showed fast diffusion and long retention in the targeted lymph node. Moreover, HFt-RFP induced strong cytotoxic $CD8^+$ T cell responses, resulting in significant inhibition of tumor growth in RFP-expressing tumor-bearing mice. Here, we show that LN-targeting strategy using antigen-presenting proteinticles holds promises for effective cancer immunotherapy.

Keywords: Lymph node-targeting; antigen-presenting proteinticles; cancer immunotherapy; cancer vaccine; T cell response; tumor regression.

Master's in pharmacy

Student number: 2013-24023

Thesis advisor: Prof. Dong Soo Lee

Table of Contents

List of Tables

List of Figures

Figure 5. Visualization of proteinticle distribution in the sectioned lymph nodes. The red color represents each particles and the nucleus was stained with DAPI (Blue). The scale bar indicates 100μm.

Figure 6. Snap shots of HFt-RFP real-time imaging. (A) Intradermal injection of Cy5.5-labelled HFt-RFP into the mouse permitted the real-time imaging of the flow of particles. 20 μL of 1 μM HFt-RFP was injected at the right forepaw and the same amount of particle was re-injected. The injection time was set as 0 s. (B) Clear image of the lymphatic vessel and the targeted lymph node. Arrow-pointed part is the lymphatic vessels and the circled part is the lymph node. Scale bar represents 4 mm.

Figure 7. Enlarged lymph node following vaccination with HFt-RFP. (A) Photographs of the lymph nodes [respective brachial (Br) and axillary (Ax) lymph nodes] removed from the mice 7 days after the final vaccination. Mice were vaccinated with PBS, RFP or HFt-RFP three times at 1-week intervals. The scale bar indicates 1 cm. (B) The volume of lymph nodes (n=3). Asterisks indicated $p < 0.005$ between HFt-RFP group and the other groups.

Figure 8. Enhanced antigen-specific immune response following vaccination with HFt-RFP. (A) Intracellular cytokine staining data followed by flow cytometry analysis depicting the number of RFP specific interferon (IFN)-γ-secreting $CD8^+$ T cells in the four groups of mice which were vaccinated with PBS, RFP, HFt, and HFt-RFP for three times at 1-week intervals. (B) Bar graph demonstrating the population of RFP-specific IFN-γ-$CD8^+$ T cells per 5 x 10^8 pooled splenocytes (mean ± s.d.).

Figure 9. *In vivo* tumor inhibition effect of HFt-RFP vaccines. (A) Vaccination schedule. (B) Representative images of tumor-bearing mice and excised tumors on day 19. Upper photographs show the RFP-expressing tumor-bearing mice vaccinated with PBS, RFP, HFt, and HFt-RFP. Dotted circles indicate tumors. Lower photographs are the tumors excised from each mouse. The scale bar indicates 1 cm. (C) Time-dependent tumor growth of mice after inoculation with RFP gene-transfected mouse melanoma cells (RFP-B16F10; n=5). C57BL/6 mice were received treatments with 10 μL of PBS (Black square), RFP (Blue circle), HFt (Gray diamond), and HFt-RFP (Red triangle) three times at 1-week intervals. Saline was used as a control group. Asterisks represent $p < 0.05$ between HFt-RFP group and the other groups. (B) Time-dependent changes in body weight after RFP-B16F10 inoculation.

Figure 10. Histological analysis of sectioned lymph nodes after immunization. (A) Immunofluorescence double-staining of the lymph nodes in mice with vaccinated with PBS, RFP, HFt, and HFt-RFP to identify the lymphocyte population of the lymph nodes. The lymph nodes are dual-stained with monoclonal mouse anti-human CD79α (Green) for B cell detection and polyclonal rabbit anti-human CD3 (Red) for T cell detection. The nucleus was stained with DAPI (Blue). The scale bar indicates 50 μm. (B) The lymphocyte cell populations of the LNs from various mice of **a** (n=6). Asterisks indicate $p < 0.05$ between T cell population of HFt-RFP group and T cell populations of the other groups.

1. Introduction

Cancer immunotherapy is a new class of cancer treatment to harness the body's own immune system to defeat cancer. Among many types of cancer immunotherapies such as antibody therapy, cytokine therapy, adoptive cell therapy, vaccination and so on, cancer vaccine therapy has been quite successful in cancer treatment [1, 2]. Cancer vaccine is a highly targeted substance designed to elicit T cell and B cell immunity. However, there are still existing hurdles to overcome for induction of specific and robust immune responses against cancer cells. For efficient activation of antigen-specific immune cells, sufficient amount of antigens should be exposed and presented on antigen-presenting cells (APCs) such dendritic cells (DCs) and macrophages for long periods of time [3]. In this respect, lymph nodes (LNs) can be potential target organs for local antigen delivery, because not only LNs contain a high population of APCs along with T cells and B cells but also it is possible to establish systemic immunity through LNs [4-6]. If antigens are locally delivered to LNs, there must be a higher chance to be exposed to APCs, and this would induce a high number of lymphocytes productions resulting in much more potent immune responses. However, tumor antigens including proteins and peptides from tumor cells are likely to show poor pharmacokinetic properties and may be quickly cleared even before they reach LNs and meet APCs [7, 8].

Various antigen delivery strategies based on nanotechnology has emerged for vaccine development due to improvements in antigen stability and immunogenicity along with slow release of antigens in the targeted site [3, 9]. Even though, many synthetic and virus-like NP have been studied for cancer, few natural NPs, including liposomes and albumin (e.g., Abraxane, Doxil) have been clinically approved. This is because synthetic NPs still possess nanotoxicity and health, safety, and environmental risks, and virus-like particles

(VLPs) are needed to develop production platform to induce post-transcriptional modifications, which are typical of viral proteins [10-12]. Recently, protein-based nanoparticles (named “proteinticle) are arising as versatile antigen delivery platform or vaccine adjuvants to induce effective immune responses against cancer [13]. Proteinticles, as natural macromolecules, possess distinct advantages over synthetic nanomaterials, such as higher biodegradability and biocompatibility along with easy surface modification through genetic or chemical methods. Also, proteinticles don’t need post-transcriptional modifications like VLPs. Therefore, it is possible to use well-established E.coli expression system, which enables high production yield with low cost [14].

Among many proteinticles being studied, human ferritin heavy chain (HFt) was selected as an antigen carrier for targeting LNs. Ferritin is a ubiquitous protein, which plays roles in iron detoxification and storage. There are two types of subunits, heavy chain and light chain, in ferritin particle, and 24 subunits are self-assembled together to form a round-shaped structure [14]. In this study, only ferritin heavy chain was used for proteinticle formation. This ferritin particle composed of 24 heavy chains has appropriate size for LN-targeting (10-80 nm) and can bind to TIM-2 receptors expressed on the surface of B and T lymphocytes [15, 16]. As a model antigen, red fluorescence protein (RFP) was genetically fused into HFt resulting in HFt-RFP monomers. As the same with HFt particle, 24 identical copies of HFt-RFP self-assembled into a spherical particle showing appropriate size for LN-targeting. Finally, the efficacy of RFP-presenting HFt in LN targeting and inhibiting the tumor growth of RFP-expressing B16F10 tumor in mice was demonstrated.

2. Materials and methods

2.1 Biosynthesis of HFt-RFP

Through polymerase chain reaction amplification using the appropriate primer, a clone encoding N-NdeI-$(His)_6$-HFt-XhoI-linker (G3SG3TG3SG3)-RFP-HindIII-C was prepared. This gene was cloned using a previously cloned expression vector, and sequentially ligated into pT7-7 plasmid to construct the expression vector pT7-HFt-RFP [14, 17, 18]. After complete sequencing, *Escherichia coli* BL21 (DE3) was transformed with the expression vector, and ampicillin-resistant transformants were selected and utilized to synthesize the HFt-RFP proteinticles.

The prepared expression vectors were transformed into *E.coli* BL21 (DE3) and then ampicillin-resistant transformants were selected. After cultivation at 20 ℃, the recombinant cells were harvested after 16 hour following 1mM isopropyl β-D-thiogalactopyranoside (IPTG) induction. The harvested recombinant cells were disrupted, and cell-free supernatant were separated from insoluble protein aggregates by centrifugation (13,000 g for 10 min). After washing the resin with binding buffer (50 mM sodium phosphate, 300 mM NaCl, 10 mM imidazole, pH 8.0), the lysate was loaded on the column and then the proteinticles were eluted using buffer (50 mM sodium phophatate, 300 mM NaCl, 250 mM imidazole, pH 8.0) after several washing steps. Eluted proteinticles were purified through a 60 % to 20 % (w/v) continuous sucrose step gradient at 24,000 rpm for 16 h at 20 ℃. Proteinticles were obtained in 50 – 60 % of sucrose phase and the buffer was exchanged with reassembly buffer using ultrafiltration.

2.2 Characterization of HFt-RFP

Size distribution and surface charge of the prepared HFt-RFP were measured using a Zetasize Nano ZS (Malvern Instruments, Ltd., Worcesterchire, UK) equipped with a 633 nm wavelength of laser. All measurements were done in triplicate. The sample was dissolved in distilled water at concentration of 1.0mg/ml and sonicated for 3 min by the probe-equipped sonicator (Ultrasonic Processor, GEX-600; Sonics & Materials. Newtown, CT) at 90 W. The morphological shape of HFt-RFP was investigated using TEM (CM-200 electron microscope, Philips, CA), operating at an acceleration voltage at 80 kV. For the preparation of TEM samples, one drop of the proteinticle suspension (1 mg/ml) was placed onto a 200-mesh copper grid which was pre-coated with carbon. After 2 min of deposition, distilled water was removed and air-dried. Negative staining was applied using a droplet of a 2% (w/v) aqueous uranyl acetate solution. In SDS-PAGE analysis, the proteinticle was mixed with a sample buffer (20 % SDS, 0.1 M Tris [pH 8.0], 1% dithiothreitol [DTT], 0.1 % [w/v] bromophenol blue, and 10 mM ethylenediaminetetraacetic acid). After boiling 10 min, the mixtures were loaded on a 15% gradient polyacrylamide gel. The gel was stained with Coomassie blue (3 %, w/v) and scanned.

2.3 Preparation of Cy5.5-labelled HFt-RFP

For *in vivo* imaging, NIR dye, Cy5.5 was labeled to HFt-RFP. Cy5.5 N-hydroxysuccinamide (NHS) ester (Cy5.5-NHS; 2 mmol, excitation and emission maximum of 675 nm and 693 nm, respectively, GE healthcare, Piscataway, NJ) was incubated with the purified HFt-RFP in sodium bicarbonate (0.1 M, pH 8.5) at room temperature for 12 h. Cy5.5-labeled proteinticle was loaded onto a sucrose step gradient (40 % (w/v), 35 %, 30 %, 25 %, and 20 %) and centrifuged at 35,000 rpm for 16 h at 4 ℃ to separate the unbound Cy5.5 from Cy5.5-labeled HFt-RFP. Subsequently, sucrose solution (20 % - 25 % sucrose) containing Cy5.5-labeled HFt-RFP was fractionated, and

then exchanged to PBS (2.7 mM KCl, 137 mM NaCl, 2 mM KH_2PO_4, 10mM Na_2HPO_4, pH7.4) by ultrafiltration (Amicon Ultra 100K, Millipore, Billerica, MA).

2.4 Lymph node accumulation

All experiments using live animals were carried out in compliance with the relevant laws and institutional guidelines of Korea Institute of Science and Technology (KIST). Male athymic nude mice of age 5 weeks (Orient, Korea) were anesthetized by intraperitoneal injection of xylazine (10 mg/kg body weight) and Zolazepam (5 mg/kg body weight). 20μl of 1μM HFt-RFP in PBS was subcutaneously injected into the right footpad of mice. *In vivo* and *ex vivo* NIR images were acquired with IVIS spectrum. For the quantitative analysis, total photon counts in the lymph nodes were measured using the region of interest (ROI) tool. The mice were sacrificed, and their brachial and axillary lymph nodes were removed and subjected to NIR fluorescence imaging. To confirm the movement of HFt-RFP into the regional LN through lymphatic vessels, real-time intravascular dynamics of Cy5.5-labeled HFt-RFP was observed in live mice using a Small Animal Imaging System (OV100, Olympus, Japan) with 620-650 nm/680-710 nm (Ex/Em) channel. Prior to recording, the mice skin around the LN was removed to develop clear flow image, and 20μL of Cy5.5-labeled HFt-RFP was subcutaneously injected at the right footpad of mice. The flow of Cy5.5-labeled HFt-RFP was recorded during 3 min post-injection.

2.5 Intracellular cytokine staining

Mice were vaccinated with PBS and 10 μM of RFP, HFt, and HFt-RFP for three times at one week intervals for maturation of T cells into memory T cells. One week after the last vaccination, spleen was excised and splenocytes were harvested from the mice using cell strainer. After PBS washing, splenocytes

were treated with RBC lysis buffer and incubated for 1 min at RT, then PBS-washed again. For intracellular cytokine staining, 5×10^6 pooled splenocytes from each immune-boosted group were activated with 1 μg/mL RFP peptide (SSLQDGTFI). In order to block cytokine release from cells, 1 μg/mL of Golgi plug (BD biosciences) were additionally treated and 1 h incubation was followed at 37 ℃. To determine IFN-γ-releasing CD8+ T cell analysis, PBS washed splenocytes were stained with CD8+ T cell antibody (BD Biosciences) for 30 min at 4 ℃. After being treated with 200 μL of Cytofix/Cytoperm (BD Biosciences) to make holes on cell membrane, cells were stained with IFN-γ antibody (BD Biosciences) and incubated for 30 min at 4 ℃. Followed by additional PBS washing, the number of RFP-specific IFN-γ-secreting CD8+ T cells was calculated by FACSCalibur flow cytometer (BD Biosciences) using CELLQuest software.

2.6 Evaluation of tumor inhibition effect

For evaluating inhibition of tumor growth, C57BL/6 mice of age 6 weeks (Orient, Korea) were subcutaneously vaccinated with 10 μL of HFt-RFP (1 μM) three times at 1-week intervals. One week after the final vaccination, the mice were subcutaneously inoculated with 5×10^5 RFP gene-transfected mouse melanoma cells (RFP-B16F10) into the flank. Tumor size was observed by measuring the minor and major axis of the tumors with electronic digital calipers. Tumor volume was calculated according to the following formula: (tumor volume) = (major axis) × (minor axis)^2 × 0.52 [28]. Mice were euthanized after tumor volumes reached 1500 mm^3. Body weight of mice was monitored.

2.7 Immunofluorescence dual-staining and lymphocytes population analysis

After three-time of boosting with PBS, RFP, HFt and HFt-RFP, lymph nodes were excised and fixed in 4% formaldehyde. Each node was dehydrated and embedded in paraffin, and sectioned at 6μm in thickness for histological evaluation. Prior to staining, the tissue sections were washed twice in xylene for 10 min each to dewax, and rehydrated step by step using an ethanol gradient from 100% to 70%. To quench the endogenous peroxidase activity, 3% Hydrogen peroxide (H_2O_2) was treated for 10 min and antigen retrieval process was performed by boiling in Tris-EDTA buffer (pH9) for 10 min. Subsequent to cooling and PBS washing, the slides were first incubated in monoclonal mouse anti-human CD79α (1:200 diluted in PBS, dakocytomation, Carpinteria, CA) for 2 h, and then PBS washing and the FITC-labeled goat anti-mouse IgG_{2b} (1:300 diluted in PBS, Santa Cruz biotechnology, Santa Cruz, CA) treatment were followed for 30 min for B cell detection. After harsh washing with PBS, further T cell staining was carried out by applying polyclonal rabbit anti-human CD3 (1:200 diluted in PBS, dakocytomation) for 2 hours which was detected by incubating the slides with CFL555-labeled mouse anti-rabbit IgG (1:300 diluted in PBS, Santa Cruz biotechnology) for 30 min. All the antibody incubation was performed at room temperature and all tissues were counterstained with 0.1μg/mL DAPI solution (4',6-Diamidino-2-phenylindole, Invitrogen) for 10 min. The stained lymph node sections were examined under IX81-ZDC focus drift compensation microscope and digital image transfer software (Olympus, Tokyo, Japan) and 8 fields (x 200) of each were randomly selected for analysis of the population of B cells and T cells. The resulted fluorescence images were analyzed using imaging analysis software (Image-Pro plus 4.1; Media Cybermetics, Silver Spring, MD) and the ratio of cell population was plotted using OriginPro8.

2.8 Statistical analysis

Data represents the means ± standard deviation. A one-way analysis of variance was used for the comparison of variables between groups. A value of $p < 0.001$ was considered statistically significant.

3. Results

3.1 Development and characterization of HFt-RFP

In the previous study, 4 types of proteinticles which fit the optimal size for uptake by lymphatic system (9 – 32 nm) were compared in lymph node targeting ability [19]: DNA-binding protein from starved cell (DPS), Proteasome from *Thermoplasma acidophilum* (PTS), Hepatitis B virus core antigen protein (HBVC) and human ferritin heavy chain (HFt). Among 4 proteinticles, HFt showed the fastest arrival and the longest retention time in the targeted lymph nodes. Based on the results, HFt was selected as a promising antigen carrier for lymph node targeting-cancer immunotherapy. As a model antigen, which is another essential part of vaccine, red fluorescent protein (RFP) was chosen.

To develop a proteinticle-based cancer vaccine, RFP-modified HFt (HFt-RFP) was synthesized from a single vector, in which the C-terminus of HFt and the N-terminus of RFP were genetically fused, affording dense display of RFP on the surface of HFt. Through simple genetic modification, RFPs were engineered to be exposed on the surface of HFt for efficient antigen exposure to antigen presenting cells (APCs). The 24 HFt monomers self-assembled to form HFt proteinticles with uniform structure and topology [14, 20]. It has been also reported that RFP-immobilized gold particles exhibited significant anti-tumor efficacy to RFP-expressing melanoma tumor-bearing animals [5]. As shown in **Fig. 1**, we planned to insert a flexible glycine-rich linker peptide (G2SG3TG3SG3) between the C-terminus of HFt and the N-terminus of RFP. This linker not only provides conformational flexibility for correct folding and self-assembly of HFt, but also helps the RFPs to be well-exposed on the surface of HFt particles [21]. Furthermore, we additionally inserted a polyhistidine tag (His_6) to the N-terminus of HFt for metal-affinity purification using Ni^{2+}. After synthesis in *E.coli*, HFt-RFP was purified from the crude cell lysates through

simple metal affinity purification, followed by sucrose gradient fractionation.

After preparing HFt-RFP, the molecular weight of HFt-RFP monomer was first analyzed and compared with RFP and HFt monomer using sodium dodecyl sulfate-polyacrylamide gel electrophoresis (SDS-PAGE) (**Fig. 2A**). The result showed that one thick band around 30 kDa with one band in RFP lane, which corresponds to the molecular weight of RFP (26.8 kDa). In HFt lane, single band was appeared at 20 kDa range, corresponding to the molecular weight of HFt monomer (21.91 kDa) and HFt-RFP lane showed one thick band around 50 kDa range and two weak bands, which were speculated as RFP-originated bands. Once the monomers are expressed, 24 monomers foregather and form a homogeneous nano-size particle structure of HFt and HFt-RFP [16]. These prepared HFt and HFt-RFP were further confirmed by dynamic light scattering (DLS) and transmission electron microscopy (TEM) to observe the shape of particles and the changes after RFP introduction to the surface of HFt (**Fig. 2B, 2C**). When compared to HFt, which was 11.7 ± 0.8 nm in a diameter, HFt-RFP had a bigger size of 25.7 ± 0.2 nm, and both showed a round shape of structure. In addition, HFt-RFP had a positive surface charge (6.58 ± 0.3 mV), as compared to the slightly negative surface charge of natural HFt (-5.69 ± 0.44 mV), due to immobilization of positively charged RFPs on the surface HFt (**Table 1**). Although the change in surface charge was observed, these results suggest that the developed HFt-RFP vaccine particle still fits to the appropriate range for efficient lymph node delivery.

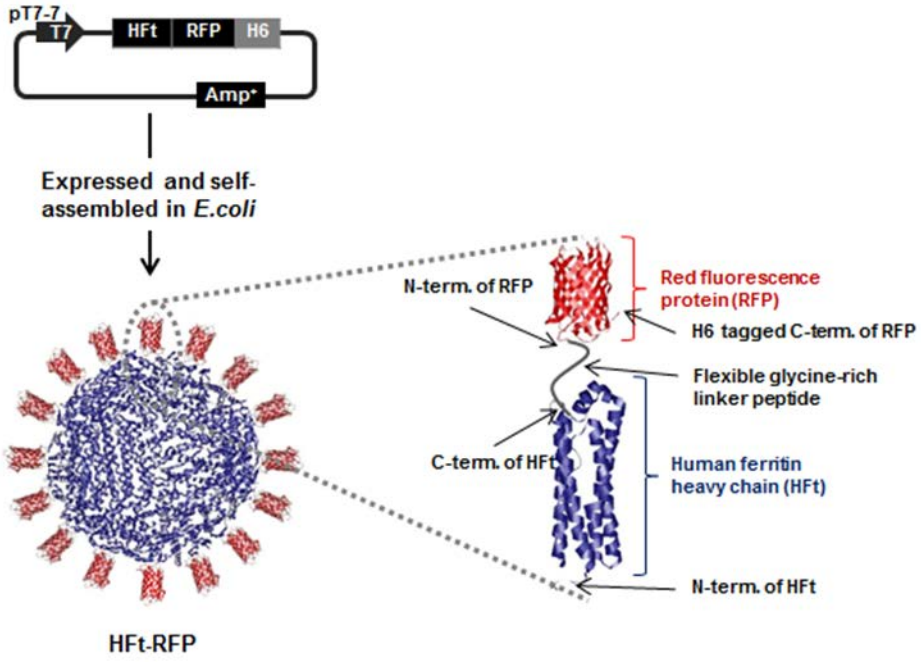

Figure 1. Development of antigen-presenting proteinticle for lymph node-targeting cancer immunotherapy. Red fluorescence protein (RFP, model tumor antigen)-modified HFt (HFt-RFP) were biosynthesized from a single vector, affording dense density of RFP on the surface of HFt.

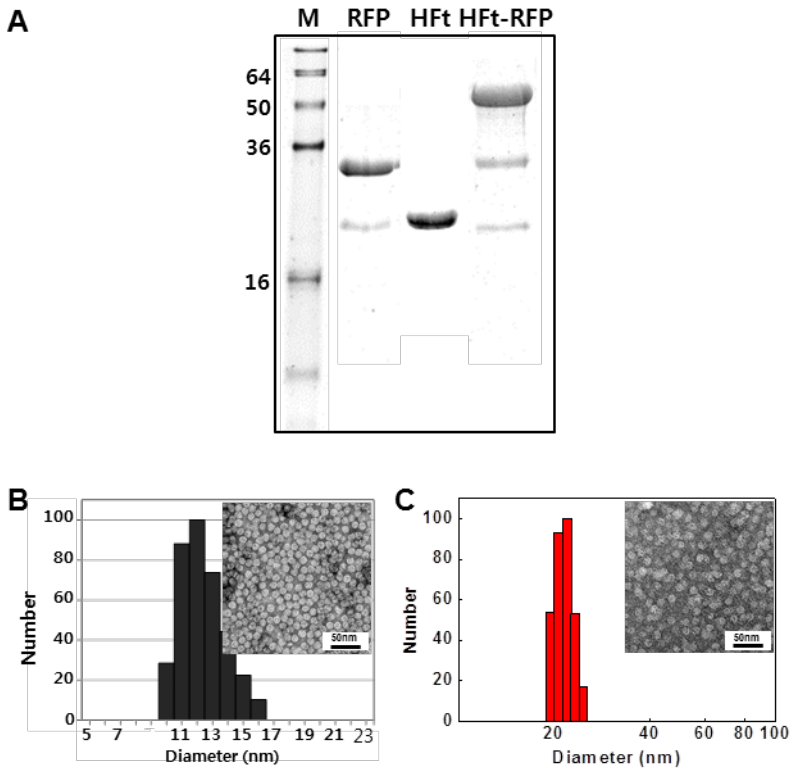

Figure 2. SDS-PAGE analysis and characterization by using DLS and TEM imaging. (A) The molecular weight of each subunit – a model antigen (RFP), a carrier (HFt), and a vaccine proteinticle (HFt-RFP) – were determined by SDS-PAGE analysis. (B, C) Size analysis and transmission electronic microscopic images of HFt (B) and HFt-RFP (C).

Table 1. Characteristics of proteinticles

	Molecular weight (kDa)[a]	Diameter (nm)[b]	Zeta potential (mV)[c]
HFt	525.84	11.7±0.8	-5.69±0.44
HFt-RFP	1169.04	25.7±0.2	6.58±0.3

[a] Average molecular weight from EXPASY
[b] Mean diameter measured by dynamic light scattering (DLS)
[c] Zeta potential measured by DLS

Table 1. Physicochemical properties of proteinticles

3.2. Comparison of HFt-RFP with RFP, HFt in time-dependent in vivo and ex vivo biodistribution.

The distinct physicochemical characteristics that may alter *in vivo* behavior of nano-sized materials can be size, shape, surface charge and flexibility of nanoparticles [22]. In particular, the size of particles is one of the important factors that may influence accumulation pattern in lymph node-targeting, due to the structural property of lymphatic system [23]. Even though the size of HFt-RFP is still with the optimal size range for lymph node-targeting, the size of HFt-RFP became twice bigger after introducing RFPs on the HFt surface, and this size incensement may affect the lymph node targeting efficacy

To investigate the difference in accumulation in the targeted lymph node area, a near-infrared (NIR) florescence dye, Cy 5.5, was used to label the surface of RFP, HFt and HFt-RFP. Cy5.5 (0.1 wt%)-labeled proteinticles presented strong NIR fluorescence intensity in phosphate buffered saline (PBS), and the proteinticle size was not altered up to 1 week, indicating the excellent stability of each proteinticles in PBS. Prior to observation, each samples had been adjusted to have the same label of fluorescence intensity and 20 μl of them was subcutaneously injected into the left forepaw of mice, then their lymph node-targeting efficacies at pre-determined times were observed using NIR fluorescence imaging device. Within 1 min post-injection, fast and accurate identification of the lymph nodes was clearly detected and the NIR fluorescence signal in the lymph nodes gradually increased up to 4 h post-injection indicating that the proteinticles migrated from the footpads to the targeted lymph node areas (**Fig. 3**). Notably, the lymph node injected with HFt-RFP showed much stronger signal compared to HFt and RFP at all the measured time points. The signal then started to decrease with similar patterns and the lymph nodes injected with RFP and HFt completely lost the fluorescence intensity. In the lymph node treated with HFt-RFP, weak signal was still produced even 120 h after injection.

Accumulation of proteinticles at target lymph nodes was also confirmed by

ex vivo fluorescence images of excised tissues (liver, lung, spleen, kidney, heart, and lymph nodes) (**Fig. 4A**). Among the tissues, we clearly observed the strongest NIR signals in the lymph nodes, as compared to other tissues, indicating that proteinticles were primarily localized lymph nodes, whereas proteinticles in normal tissues were negligible. In comparison of treated lymph nodes, the NIR signals were observed in the proximal lymph nodes (injection side), but no in the distal lymph nodes, suggesting local delivery of the proteinticles after subcutaneous injection (**Fig. 4B**). As expected, HFt-RFP-treated lymph nodes exhibited the highest NIR fluorescence signal, as compared to PBS, RFP and HFt injected lymph nodes, and this result indicates the lymph node-specific targeting efficacy of HFt-RFP decisively.

We also performed histological fluorescence imaging of the dissected LNs 4 h post-injection. The fluorescence signals were observed sectioned lymph nodes which were treated with RFP, HFt and HFt-RFP (**Fig. 5**). However, the brightest fluorescence signal was detected in the HFt-RFP injected lymph node, corresponding to the precedent results.

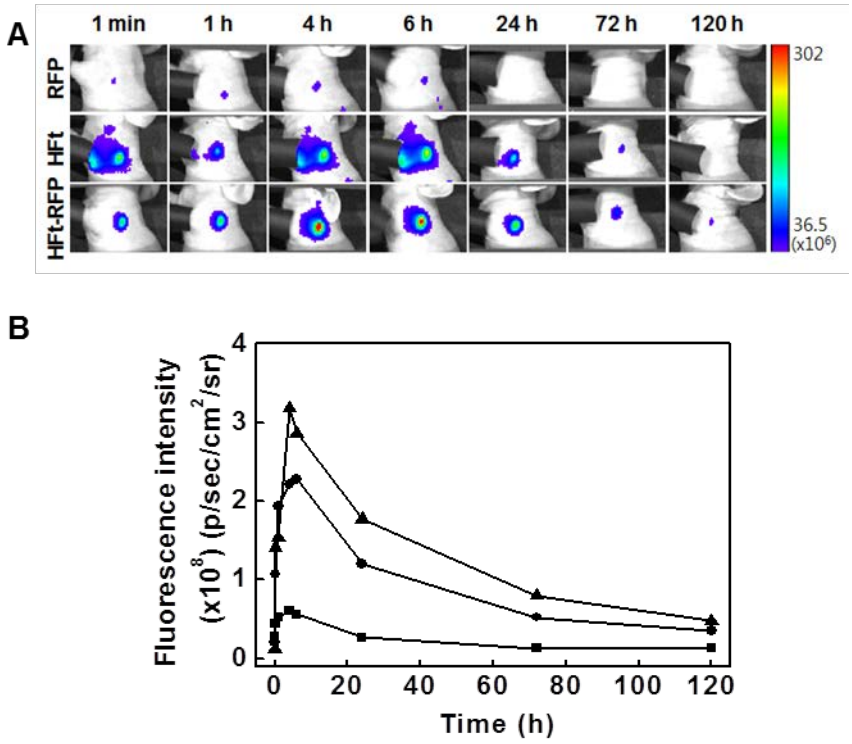

Figure 3. Time-dependent biodistribution of RFP, HFt, and HFt-RFP in the targeted lymph nodes. (A) Time-course fluorescence intensity in the lymph node regions. During 120 h, the near-infrared (NIR) fluorescence intensity was measured at pre-determined time after subcutaneous injection of RFP, HFt, and HFt-RFP. (B) The plotted graph with the fluorescence intensity at each time points.

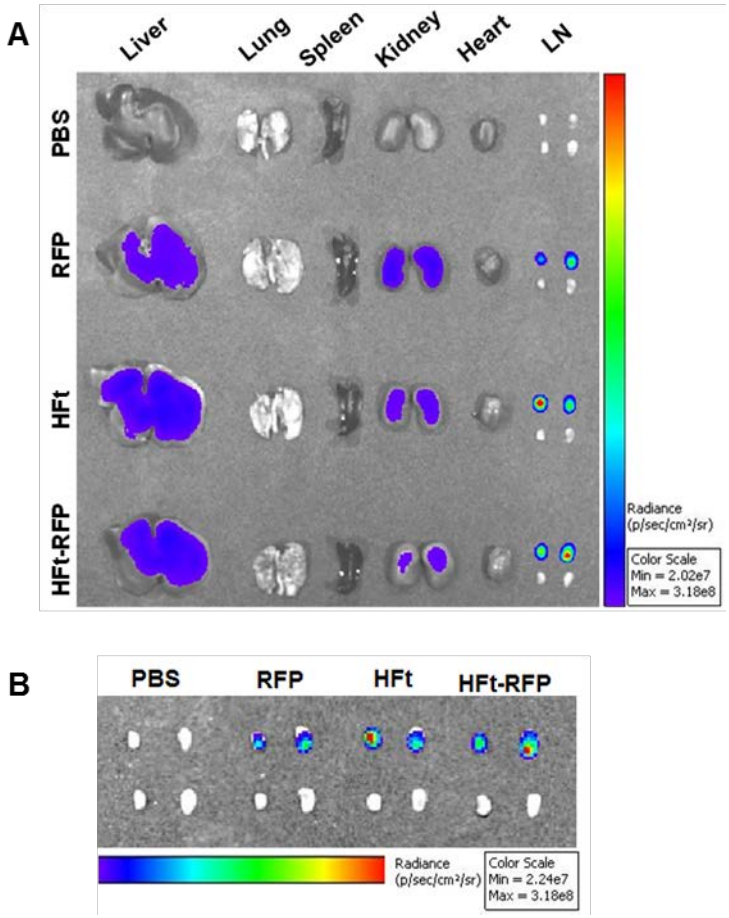

Figure 4. *Ex vivo* fluorescence images. (A) *Ex vivo* fluorescence images of liver, lung, spleen, kidney, heart, and lymph node after subcutaneous injection of PBS, RFP, HFt, and HFt-RFP. (B) Fluorescence images of excised proximal (injection side) and distal lymph nodes. All of organs were excised 4 h post-injection.

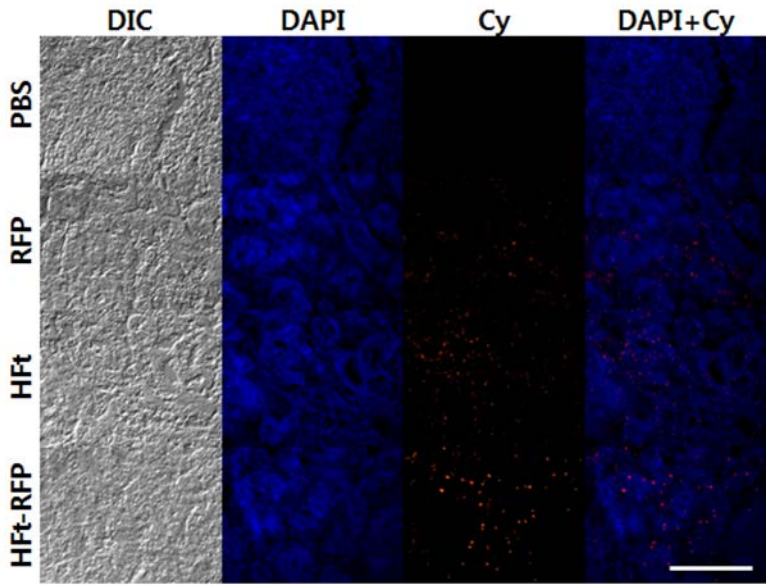

Figure 5. Visualization of proteinticle distribution in the sectioned lymph nodes. The red color represents each particles and the nucleus was stained with DAPI (Blue). The scale bar indicates 100μm.

3.3. Real-time tracking of HFt-RFP to the regional lymph node

When compared to RFP and HFt, HFt-RFP showed better lymph node targeting efficacy as expected. To visualize the movement of HFt-RFP particles toward the targeted lymph node, real-time intravascular dynamics of Cy5.5-labelled HFt-RFP was observed in live mice (**Fig. 6A, 6B**). The skin of the mice was removed for better observation of the lymphatic vessel and the lymph node, and 20 μl of HFt-RFP was subcutaneously injected at the right footpad. Right after the local injection, HFt-RFP visualized a lymphatic vessel with fast migration, and the position of brachial lymph node was further identified within 30 s. When the same amount of HFt-RFP was re-injected, much clearer picture of the lymph nodes was observed, and it also took around 30 s for the additionally delivered particles to the targeted lymph node. This result also supports that HFt-RFP has a great lymph node-targeting efficacy and suggests that RFP antigen carried by HFt has higher chances to be exposed by APCs in the targeted lymph node.

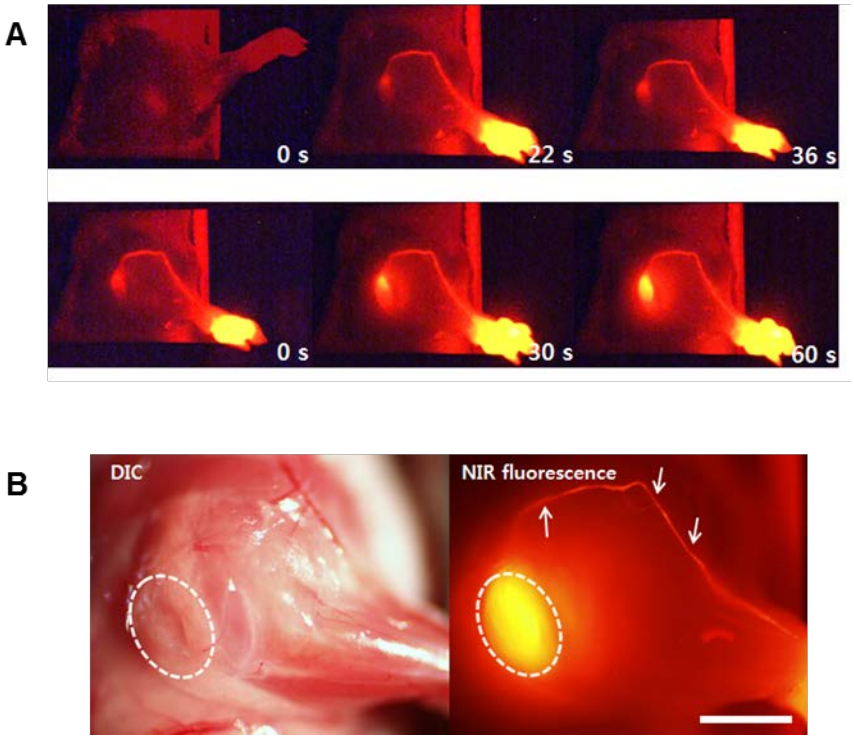

Figure 6. Snap shots of HFt-RFP real-time imaging. (A) Intradermal injection of Cy5.5-labelled HFt-RFP into the mouse permitted the real-time imaging of the flow of particles. 20 μL of 1 μM HFt-RFP was injected at the right forepaw and the same amount of particle was re-injected. The injection time was set as 0 s. (B) Clear image of the lymphatic vessel and the targeted lymph node. Arrow-pointed part is the lymphatic vessels and the circled part is the lymph node. Scale bar represents 4 mm.

3.4 Model tumor antigen-displaying proteinticles as an immunotherapeutic vaccine

To understand the immune response of mice after vaccination, changes in the lymph node were comparatively analyzed in mice vaccinated with PBS, RFP, HFt, and HFt-RFP. We first compared the volumes of the lymph nodes after vaccination. The average volume of the lymph nodes increased in mice that were vaccinated with RFP (3.89mm^3), HFt 9.23 mm^3), and HFt-RFP (13.31 mm^3), when compared with those that received PBS treatment (1.26 mm^3). In particular, mice vaccinated with HFt-RFP had significantly larger sized lymph nodes than other groups (**Fig. 7A, 7B**; $p < 0.05$), suggesting active immune responses in the regional lymph nodes.

To investigate whether HFt-RFP could elicit the antigen-specific immune responses capable of producing anti-tumor effects, the strength of the $CD8^+$ T cell response was assessed in vaccinated mice. C57BL/6 mice were subcutaneously vaccinated with HFt-RFP (10 μM), RFP (10 μM), HFt (10 μM), and PBS three times at 1-week intervals. Seven days after the final vaccination, splenocytes were activated *ex vivo* with the RFP (SSLQDGCFI, 111-119) peptide, which acts as an epitope for RFP primed response [24]. The strength of the $CD8^+$ T cells in the spleen. The number of IFN-γ-secreting $CD8^+$ T cells observed in the spleens of mice vaccinated with HFt-RFP (85 ± 4) was approximately 2.93-fold higher than mice vaccinated with PBS (26 ± 5), RFP (29 ± 4), or HFt (32 ± 3; $p < 0.002$; **Fig. 8A, 8B**). These data suggest that HFt-RFP stimulates antigen-specific cellular responses, which induce the production of cytotoxic T cells.

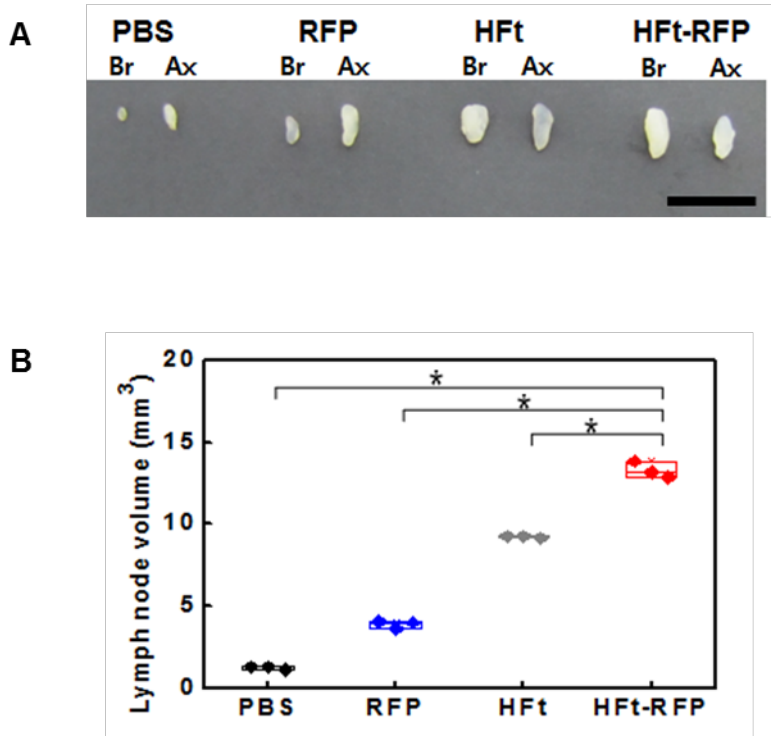

Figure 7. Enlarged lymph node following vaccination with HFt-RFP. (A) Photographs of the lymph nodes [respective brachial (Br) and axillary (Ax) lymph nodes] removed from the mice 7 days after the final vaccination. Mice were vaccinated with PBS, RFP or HFt-RFP three times at 1-week intervals. The scale bar indicates 1 cm. (B) The volume of lymph nodes (n=3). Asterisks indicated $p < 0.005$ between HFt-RFP group and the other groups.

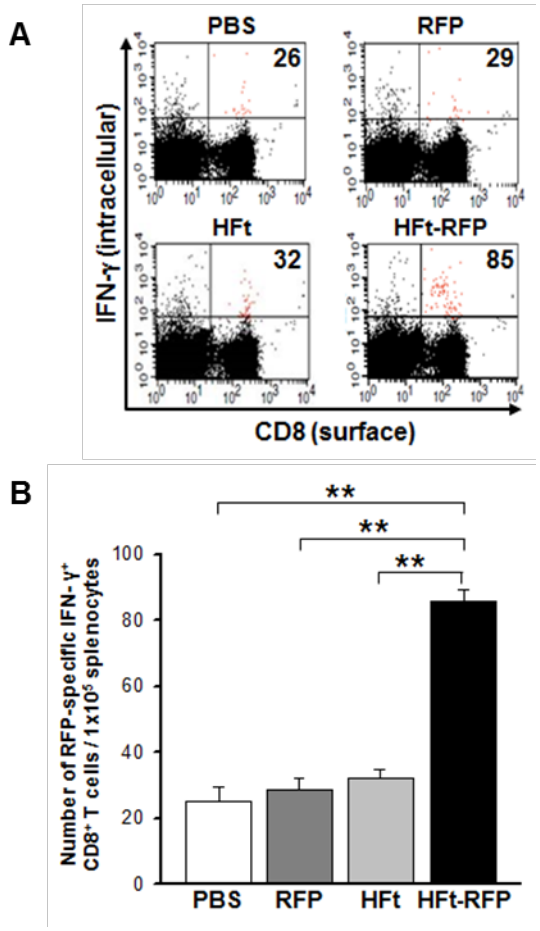

Figure 8. Enhanced antigen-specific immune response following vaccination with HFt-RFP. (A) Intracellular cytokine staining data followed by flow cytometry analysis depicting the number of RFP specific interferon (IFN)-γ-secreting $CD8^+$ T cells in the four groups of mice which were vaccinated with PBS, RFP, HFt, and HFt-RFP for three times at 1-week intervals. (B) Bar graph demonstrating the population of RFP-specific IFN-γ-$CD8^+$ T cells per 5 x 10^8 pooled splenocytes (mean ± s.d.).

3.5 In vivo anti-tumor effect

To evaluate HFt-RFP-mediated inhibition of tumor growth *in vivo*, C57BL/6 mice were subcutaneously vaccinated with HFt-RFP (10 μM), RFP (10 μM), HFt (10 μM), or PBS three times at 1-week intervals (**Fig. 9A**). Compared to RFP-, HFt-, and PBS-treated mice, which displayed rapid increases in tumor volume, the excised tumors treated with HFt-RFP showed significant decreases in tumor size 19 days after injection (**Fig. 9B**). Moreover, significant inhibition of tumor growth was observed in mice treated with HFt-RFP up to 24 days, whereas the tumor volume of the RFP-, HFt-, and PBS-treated mice reached 1500 mm^3(**Fig. 9C**; $p < 0.05$). The groups did not display significant differences in body weight, suggesting that treatment with HFt-RFP was non-toxic (**Fig. 9D**).

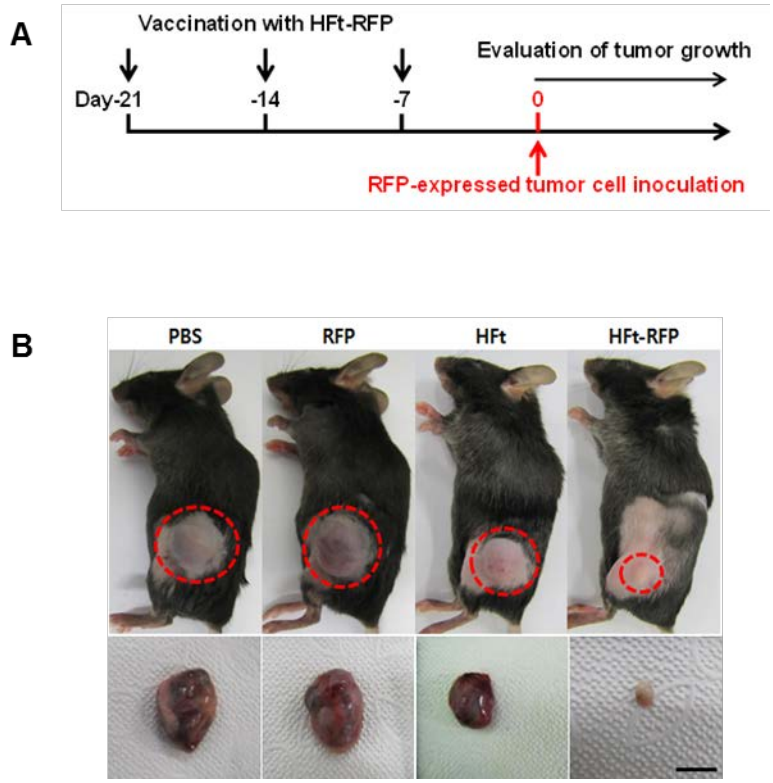

Figure 9. *In vivo* tumor inhibition effect of HFt-RFP vaccines. (A) Vaccination schedule. (B) Representative images of tumor-bearing mice and excised tumors on day 19. Upper photographs show the RFP-expressing tumor-bearing mice vaccinated with PBS, RFP, HFt, and HFt-RFP. Dotted circles indicate tumors. Lower photographs are the tumors excised from each mouse. The scale bar indicates 1 cm.

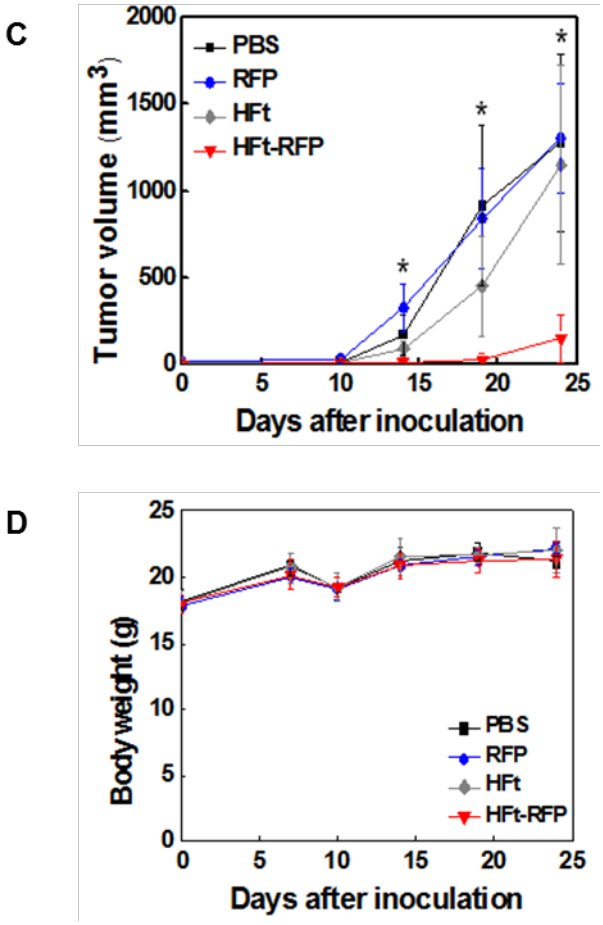

Figure 9. *In vivo* tumor inhibition effect of HFt-RFP vaccines. (C) Time-dependent tumor growth of mice after inoculation with RFP gene-transfected mouse melanoma cells (RFP-B16F10; *n*=5). C57BL/6 mice were received treatments with 10 μL of PBS (Black square), RFP (Blue circle), HFt (Gray diamond), and HFt-RFP (Red triangle) three times at 1-week intervals. Saline was used as a control group. Asterisks represent $p < 0.05$ between HFt-RFP group and the other groups. (B) Time-dependent changes in body weight after RFP-B16F10 inoculation.

3.6 Histological analysis

The profile of cell proliferation in lymph nodes changes depending on a type of antigen introduced to lymph nodes. This change determines which lymphocytes take the priority in immune response against the antigen. It is generally regarded that immune responses by T cells result in better result in cancer treatment.

To elucidate the immune response by repetitive injection of HFt-RFP vaccine, the lymphocyte population of the LN was comparatively analyzed with PBS, RFP and HFt-injected LNs. The cell population in the regional LN of PBS-treated mice comprised 54.4 ± 17.4% of B cells and 45.6 ± 17.4% of T cells. T cell populations of LNs in mice vaccinated with RFP (68 ± 8.9%), HFt (62.1 ± 9.7%), and HFt-RFP (78.9 ± 7.9%) showed an increase. This result shows that the injection of proteinticles leads the T cell predominance population change in the LNs. Specifically, the ratio of T cells in LNs vaccinated with HFt-RFP significantly increased among proteinticle-injected LNs (**Fig. 10A, 10B**; $p < 0.05$) and this supports the good outcome in the tumor regression experiment.

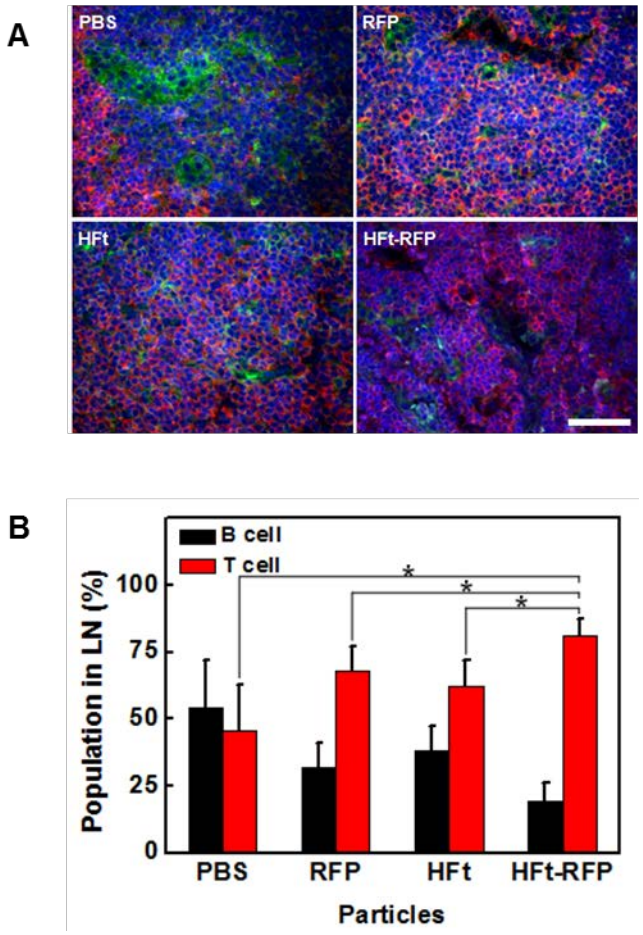

Figure 10. Histological analysis of sectioned lymph nodes after immunization. (A) Immunofluorescence double-staining of the lymph nodes in mice with vaccinated with PBS, RFP, HFt, and HFt-RFP to identify the lymphocyte population of the lymph nodes. The lymph nodes are dual-stained with monoclonal mouse anti-human CD79α (Green) for B cell detection and polyclonal rabbit anti-human CD3 (Red) for T cell detection. The nucleus was stained with DAPI (Blue). The scale bar indicates 50 μm. (B) The lymphocyte cell populations of the LNs from various mice of **a** (n=6). Asterisks indicate $p < 0.05$ between T cell population of HFt-RFP group and T cell populations of the other groups.

4. Discussion

To induce potent immune responses against cancer, a strategy of local delivery of tumor antigens to lymph nodes (LNs) was adopted for cancer immunotherapy. Not only LNs have a high population of immune cells, but also they are responsible for both cellular and humoral immune reaction [5]. Herein, we used protein based nanoparticles (proteinticles) which are self-assembled inside cells and also suggest a variety of genetic or chemical modifications. For development of a vaccine particle, human ferritin heavy chain (HFt) was selected as a potential LN-targeting carrier for antigens, and a model antigen, red fluorescence proteins (RFPs) were genetically introduced to the surface of HFt proteinticles (**Fig. 1**). Cy5.5-labelled RFP-possessing HFt (HFt-RFP) was observed *in vivo* for 120 h after subcutaneous injection and LN-targeting efficacy of HFt-RFP was evaluated (**Fig. 3**). In the additionally performed real-time imaging with Cy5.5-labelled HFt-RFP, rapid migration to the targeted LN via lymphatic vessels was visualized, and it implies that the higher probability of vaccine particles to be encountered with immune cells. Recent studies suggest that several days of antigen and adjuvant exposure to the immune system amplified the immunogenicity of a vaccine [25-27]. Thus, rapid localization and prolonged accumulation of HFt-RFP is preferable for the enhancement of antigen presentation in antigen presenting cells, which elicits cytotoxic T cell responses.

Cancer vaccines may involve either humoral or cell-mediated immune responses [28-30]. In particular, the cellular immune response, which responds to antigens displayed on tumor cells and involves mostly T cells, has been considered highly important for development of cancer vaccine [29]. After vaccination with HFt-RFP, the mean volume of regional LNs significantly increased with successful tumor inhibition, suggesting active immune responses at regional LNs (**Fig. 7A, 7B**). In addition, we found that the T cell population

in the LNs was significantly increased in the HFt-RFP-treated group (78.9 ± 7.9%) compared with the PBS-treated group (45.6 ± 17.4%; **Fig. 10A, 10B**). This suggests that the LN cell population shifted toward a T cell predominance, which is likely attributed to the expansion of the T cell zone in LNs. These results suggest that vaccination with HFt-RFP could reinforce the immune system, especially for the cell-mediated immune response. Additionally, the increased number of IFN-γ-secreting $CD8^+$ T cells supports the fact that HFt-RFP could facilitate the antigen-specific T cell response after LN targeting (**Fig. 8A, 8B**). Thus, our HFt-RFP vaccines have the potential to induce immunological T cell responses against specific antigens of tumor cells for effective immunotherapy.

In the tumor inhibition experiment, we used RFP-transfected B16F10 tumor model to characterize the tumor regression effects of HFt-RFP in mice. The encouraging antitumor results from the mice group treated HFt-RFP was observed up to 24 days (**Fig. 9A - 9D**). Taken together, the experimental results ensure the boosted immune responses and antitumor effects by HFt-RFP, a promising platform in cancer vaccine development.

5. Conclusion

Efficient delivery of antigens into LNs is essential for eliciting immune responses that eventually attack tumor cells. Human ferritin heavy chain (HFt) modified with a model antigen RFP (HFt-RFP) was effectively delivered to the target LNs, which significantly increased the size of LNs and the T cell population in LNs compared with control groups. Importantly, HFt-RFP significantly inhibited the tumor growth in RFP-expressing tumor-bearing mice for up to 24 days, as compared to free RFP antigen. Although RFP was used as a model antigen for proof-of-concept in this study, it can be switched with other tumor antigens. This approach to cancer treatment, which employs enhanced tumor-specific immunogenicity using genetically engineered proteinticles, seems to have great potentials for efficient LN-targeting and cancer immunotherapy

6. References

[1] Emens LA. Cancer vaccines: on the threshold of success. Expert Opin Emerg Drugs. 2008;13:295-308.

[2] Snook AE, Waldman SA. Advances in cancer immunotherapy. Discov Med. 2013;15:120-5.

[3] Sasada T, Yamada A, Noguchi M, Itoh K. Personalized peptide vaccine for treatment of advanced cancer. Curr Med Chem. 2014;21:2332-45.

[4] Jeanbart L, Ballester M, de Titta A, Corthesy P, Romero P, Hubbell JA, et al. Enhancing efficacy of anticancer vaccines by targeted delivery to tumor-draining lymph nodes. Cancer Immunol Res. 2014;2:436-47.

[5] Lee IH, Kwon HK, An S, Kim D, Kim S, Yu MK, et al. Imageable antigen-presenting gold nanoparticle vaccines for effective cancer immunotherapy *in vivo*. Angew Chem Int Ed Engl. 2012;51:8800-5.

[6] Shu S, Cochran AJ, Huang RR, Morton DL, Maecker HT. Immune responses in the draining lymph nodes against cancer: implications for immunotherapy. Cancer Metastasis Rev. 2006;25:233-42.

[7] Mellman I, Coukos G, Dranoff G. Cancer immunotherapy comes of age. Nature. 2011;480:480-9.

[8] Xu Z, Ramishetti S, Tseng YC, Guo S, Wang Y, Huang L. Multifunctional nanoparticles co-delivering Trp2 peptide and CpG adjuvant induce potent cytotoxic T-lymphocyte response against melanoma and its lung metastasis. J Control Release. 2013;172:259-65.

[9] Zhao L, Seth A, Wibowo N, Zhao CX, Mitter N, Yu C, et al. Nanoparticle vaccines. Vaccine. 2014;32:327-37.

[10] Chen Q, Lai H. Plant-derived virus-like particles as vaccines. Hum Vaccin Immunother. 2013;9:26-49.

[11] Council NR. A research strategy for environmental, health, and safety aspects of engineered nanomaterials. The national academies press. 2012.

[12] Kanekiyo M, Wei CJ, Yassine HM, McTamney PM, Boyington JC, Whittle JR, et al. Self-assembling influenza nanoparticle vaccines elicit broadly neutralizing H1N1 antibodies. Nature. 2013;499:102-6.

[13] Jahanshahi M, Babaei Z. Protein nanoparticle: A unique system as drug delivery vehicles. African Journal of Biotechnology. 2008;7:4926-34.

[14] Kim SE, Ahn KY, Park JS, Kim KR, Lee KE, Han SS, et al. Fluorescent ferritin nanoparticles and application to the aptamer sensor. Anal Chem. 2011;83:5834-43.

[15] Cobaleda-Siles M, Henriksen-Lacey M, Ruiz de Angulo A, Bernecker A, Gomez Vallejo V, Szczupak B, et al. An iron oxide nanocarrier for dsRNA to target lymph nodes and strongly activate cells of the immune system. Small. 2014;10:5054-67.

[16] Li L, Fang CJ, Ryan JC, Niemi EC, Lebron JA, Bjorkman PJ, et al. Binding and uptake of H-ferritin are mediated by human transferrin receptor-1. Proc Natl Acad Sci U S A. 2010;107:3505-10.

[17] Lee EJ, Ahn KY, Lee JH, Park JS, Song JA, Sim SJ, et al. A novel bioassay platform using ferritin-based nanoprobe hydrogel. Adv Mater. 2012;24:4739-44, 0.

[18] Ahn KY, Ko HK, Lee BR, Lee EJ, Lee JH, Byun Y, et al. Engineered protein nanoparticles for *in vivo* tumor detection. Biomaterials. 2014;35:6422-9.

[19] Kemnade JO, Seethammagari M, Narayanan P, Levitt JM, McCormick AA, Spencer DM. Off-the-shelf adenoviral-mediated immunotherapy via bicistronic expression of tumor antigen and iMyD88/CD40 adjuvant. Mol Ther. 2012;20:1462-71.

[20] Luzzago A, Cesareni G. Isolation of point mutations that affect the folding of the H chain of human ferritin in E.coli. EMBO J. 1989;8:569-76.

[21] Yoo L, Park JS, Kwon KC, Kim SE, Jin X, Kim H, et al. Fluorescent viral nanoparticles with stable *in vitro* and *in vivo* activity. Biomaterials. 2012;33:6194-200.

[22] Longmire MR, Ogawa M, Choyke PL, Kobayashi H. Biologically optimized nanosized molecules and particles: more than just size. Bioconjug Chem. 2011;22:993-1000.

[23] Swartz MA. The physiology of the lymphatic system. Adv Drug Deliv Rev. 2001;50:3-20.

[24] Davey GM, Mueller SN, van Vliet C, Gigowski M, Zaid A, Davies B, et al. Identification of a MHC I-restricted epitope of DsRed in C57BL/6 mice. Mol Immunol. 2013;53:450-2.

[25] Bachmann MF, Beerli RR, Agnellini P, Wolint P, Schwarz K, Oxenius A. Long-lived memory CD8+ T cells are programmed by prolonged antigen exposure and low levels of cellular activation. Eur J Immunol. 2006;36:842-54.

[26] Jewell CM, Lopez SC, Irvine DJ. In situ engineering of the lymph node microenvironment via intranodal injection of adjuvant-releasing polymer particles. Proc Natl Acad Sci U S A. 2011;108:15745-50.

[27] Shaulov A, Murali-Krishna K. CD8 T cell expansion and memory differentiation are facilitated by simultaneous and sustained exposure to antigenic and inflammatory milieu. J Immunol. 2008;180:1131-8.

[28] Li G, Andreansky S, Helguera G, Sepassi M, Janikashvili N, Cantrell J, et al. A chaperone protein-enriched tumor cell lysate vaccine generates protective humoral immunity in a mouse breast cancer model. Mol Cancer Ther. 2008;7:721-9.

[29] Dermime S, Armstrong A, Hawkins RE, Stern PL. Cancer vaccines and immunotherapy. Br Med Bull. 2002;62:149-62.

[30] Palucka K, Banchereau J. Cancer immunotherapy via dendritic cells. Nat Rev Cancer. 2012;12:265-77.

국문초록

암 면역치료법이란 우리 몸의 면역시스템을 이용하여 암에 대항하는 새로운 형태의 치료법이다. 본 학위 논문은 다양한 종류의 면역치료법 중, 항원에 대한 특이적인 면역 반응을 일으킬 수 있는 암 백신 연구에 대한 내용을 담고 있다. 암 세포에 대한 면역 반응을 일으키기 위해서는 충분한 양의 항원들이 수지상세포, 대식세포와 같은 항원제시세포에게 노출되어야 한다. 이러한 이유로, 림프절로의 국소적인 항원 전달은 강력한 면역 반응을 일으키는데 있어 적절한 전략이 될 수 있는데, 이는 많은 수의 항원제시세포, T 세포, B 세포들이 림프절에 존재하기 때문이다. 하지만 암 세포에서 유래된 단백질 또는 펩타이드와 같은 항원들은 적절하지 않은 약동학 특성을 가지고 있고, 림프절에 도달해 항원제시세포에게 노출되기 전에 몸에서 빠르게 배출될 수 있다는 단점들이 있다. 이러한 부분을 극복하기 위한 방법으로, 나노기술 기반의 다양한 입자들이 항원의 안정성과 면역원성을 개선시키기 위한 대안으로 제시되고 있다. 이 중에서 천연 고분자인 단백질을 기반으로 하는 나노입자가 효과적인 면역 반응을 일으키기 위한 항원 전달 플랫폼으로 새로이 떠오르고 있다. 단백질 나노입자는 합성 나노입자들과 비교해 보았을 때, 생분해성과 생체적합성이 뛰어날 뿐만 아니라 유전적, 화학적 방법을 통해 표면 개질이 용이하다는 장점이 있다. 본 연구에서는, 사람 유래의 페리틴 H 사슬 단백질 (Human ferritin heavy chain, HFt)과 적색형광단백질 (Red fluorescence protein, RFP)을 유망한 항원 전달체와 모델 항원으로 선정하였다. 유전적으로 재조합 된 26 nm 크기의 HFt-RFP 입자는 표적 림프절로의 빠른 확산과 림프절에서의 긴 잔류시간을 보였다. 주기적인 HFt-RFP 백신 접종은 강력하고 항원 특이적인 T 세포 반응을 유도하였고, 모

델항원을 발현하는 암을 지닌 쥐에서의 암 성장을 현저하게 저해시켰다. 이러한 결과들은 효과적인 암 면역 치료법에서 항원 제시형 단백질 나노입자를 이용한 림프절 표적화 전략의 잠재적인 가능성을 뒷받침 한다.

주요어 : 림프절 표적화; 항원 제시형 단백질 나노입자; 암 면역치료법; 항암 백신; T 세포 반응

학번 : 2013-24023